Physiological fluid dynamics

N. A. HILL

Department of Mathematics
University of Glasgow
Glasgow, G12 8QW, Scotland, U.K.
`n.a.hill@maths.gla.ac.uk`

1. Large blood vessels

1.1. Introduction – the cardiovascular system

The heart is a pump that circulates blood to the lungs for oxygenation (pulmonary circulation) and then throughout the systemic arterial system with a total cycle time of about one minute. From the left ventricle of the heart, blood is pumped into the aorta, which in adult humans has a diameter of about 2.5 cm and has a complex three-dimensional geometry. The three coronary arteries branch directly off the aorta to supply the heart. Daughter arteries branch directly from the aorta with further divisions ultimately down to the smallest blood vessels, the capillaries, in which the main exchange processes between the blood and tissues take place.

The blood returns via venules through a converging system of veins.

Arteries

The walls of the arteries have a three-layer structure made of similar materials but in different proportions resulting in different mechanical properties (Fig. 1).

I. *The intima* – lined with a single layer of cells called the endothelium, where atherosclerotic plaques first develop.

II. *The media* – consists of multiple layers of an elastic material, elastin, whose direction changes radially, separated by thin layers of connective tissue, collagen, with a few muscle cells.

III. *The adventitia* – loose connective tissue of elastin and collagen fibres.
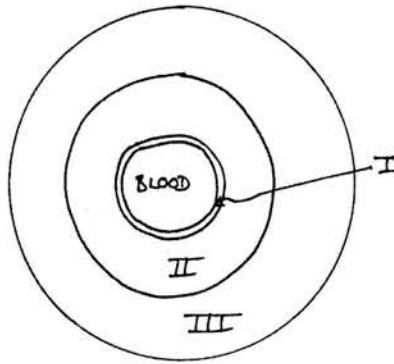
FIGURE 1. Structure of the arterial wall.

The media is structurally most important and renders the arteries to be pre-stressed, non-linearly elastic tubes.

Blood

Blood consists of cells in plasma, which is a fluid with a viscosity of

$$\mu_p \approx 1.2 - 1.6 \cdot 10^{-3} \, \mathrm{kg \, m^{-1} \, s^{-1}}.$$

45% by volume of blood consist of red blood cells which are very deformable biconcave disks with viscous contents (Fig. 2). They may aggregate.
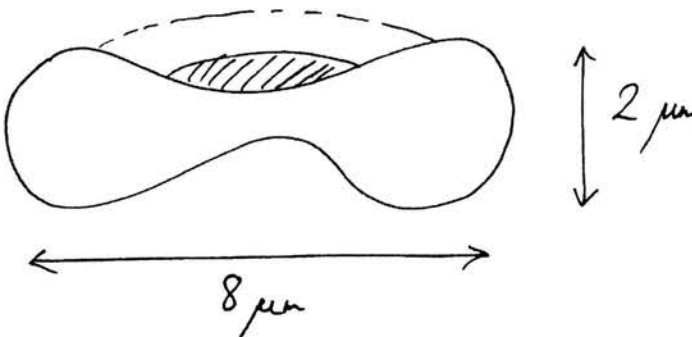

FIGURE 2. A red blood cell.

Viscosity

For shear rates $> 100\,\text{s}^{-1}$, the fluid is approximately Newtonian, with viscosity

$$\mu \approx 4 \cdot 10^{-3}\,\text{kg}\,\text{m}^{-1}\,\text{s}^{-1} \text{ at } 37°\text{C}$$

and denisty

$$\rho \approx 1.05 \cdot 10^{3}\,\text{kg}\,\text{m}^{-3}.$$

In the arteries and veins, with diameters $> 100\,\mu\text{m}$, blood can be treated as homogeneous and Newtonian.

1.2. One-dimensional theory of pulse propagation in arteries

We want to explain the mechanism and speed of propagation, changes in the shape of the pressure waveform (peaking and steepening downstream) and of the velocity waveform.

Consider an infinitely long, distensible tube of uniform undisturbed area, A_0, containing an incompressible, inviscid fluid of density, ρ. Assume the wavelengths of the disturbances $\gg$ diameter of the tube which implies that velocity profile is flat and lateral velocities can be neglected (Figs. 3 and 4).
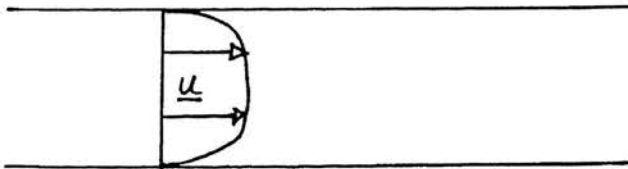

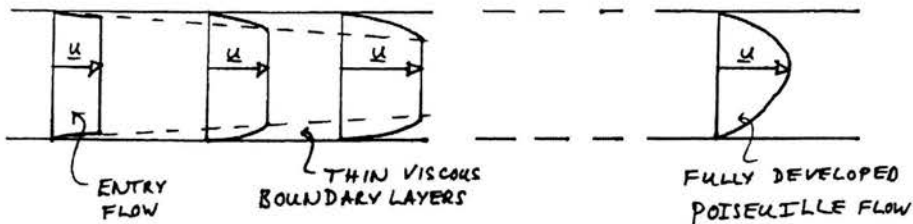FIGURE 3. Observed velocity profiles are flat, entry-type flows.

FIGURE 4. Development of entry flow.

Variables:

- $p(x, t)$ – excess pressure,
- $A(x, t)$ – area,
- $u(x, t)\,\mathbf{i}$ – cross–sectionally averaged fluid velocity.

1.2.1. Conservation of mass.

Consider a small region of the pipe between x and $x + \delta x$ (Fig. 5). In time δt, the net flux into the region is approximately

$$\rho \left[(uA)\,|_x - (uA)\,|_{x+\delta x}\right] \delta t$$

and the resulting change in mass is approximately

$$\rho \left[A\left(x, t + \delta t\right) - A\left(x, t\right)\right] \delta x.$$

Equating these gives

$$\frac{(uA)\,|_x - (uA)\,|_{x+\delta x}}{\delta x} = \frac{A\left(x, t + \delta t\right) - A\left(x, t\right)}{\delta t}$$

and, as $\delta t,\ \delta x \longrightarrow 0$, we get

$$\frac{\partial A}{\partial t} + \frac{\partial}{\partial x}(uA) = 0. \tag{1.1}$$
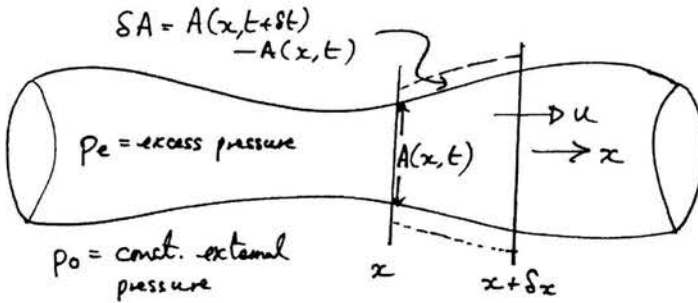

FIGURE 5. Conservation of mass sketch.

1.2.2. Conservation of momentum.

Directly from the Navier–Stokes equations on setting $\mathbf{u} = u(x, t)\mathbf{i}$ and the Reynolds number $\mathrm{R} = \infty$, we have

$$\frac{\partial u}{\partial t} + u\frac{\partial u}{\partial x} + \frac{1}{\rho}\frac{\partial p}{\partial x} = 0. \tag{1.2}$$

1.2.3. Constitutive relation.

$$p \equiv p_e - p_0 = P(A) = \text{transmural pressure},$$ (1.3)

i.e. pressure is a function of the cross-sectional area.

1.2.4. Linear theory. For small amplitude disturbances, let

$$A = A_0 + a, \quad |a| \ll A_0, \quad |u| \ll 1$$

and note that from Eq. (1.3)

$$\frac{\partial p}{\partial t} = P'(A_0)\frac{\partial a}{\partial t} + 0(a^2).$$

Equations (1.1) and (1.2) give

$$\frac{1}{A_0 P'(A_0)} \frac{\partial p}{\partial t} + \frac{\partial u}{\partial x} = 0,$$

$$\frac{\partial u}{\partial t} + \frac{1}{\rho}\frac{\partial p}{\partial x} = 0,$$ (1.4)

on neglecting small quantities. Eliminating u gives

$$\frac{\partial^2 p}{\partial t^2} = c_0^2 \frac{\partial^2 p}{\partial x^2},$$ (1.5)

where

$$c_0^2 = (\rho D_0)^{-1}$$ (1.6)

and

$$\frac{d}{dp}\left(\frac{a}{A_0}\right) = \frac{1}{D_0}$$

or equivalently

$$D_0 = \frac{1}{A_0 P'(A_0)},$$ (1.7)

is the distensibility of the tube. Equation (1.5) is the wave equation and has solutions

$$\text{with:} \quad \begin{cases} p = f(x \pm c_0 t), \\ u = \mp (\rho c_0)^{-1} f(x \pm c_0 t), \\ a = A_0 (\rho c_0^2)^{-1} f(x \pm c_0 t), \end{cases}$$ (1.8)

representing waves propagating with speed c_0. This linearisation is valid provided $| u | \ll c_0$. c_0 can be estimated from values of Young's modulus, E, for arteries (Fig. 6).
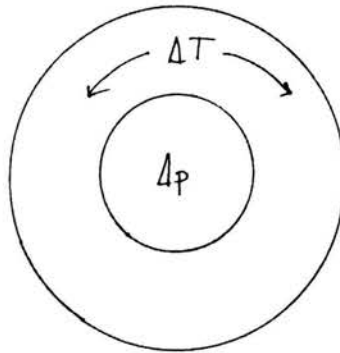
FIGURE 6. Idea: increase in pressure $\triangle p$ leads to increase in hoop tension $\triangle T$.
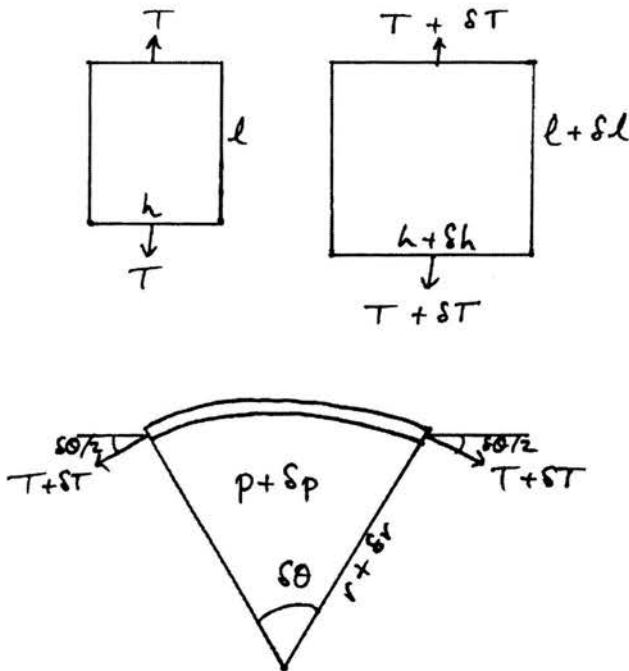

FIGURE 7. Definition sketch for Young's modulus.

(Effective, incremental) Young's modulus (see Fig. 7):

$$\delta T = Eh\frac{\delta \ell}{\ell} + O\left(\delta h\frac{\delta \ell}{\ell}\right).$$

Resolving radially (per unit length) over angle $\delta\theta$,

$$2\,\delta T \sin(\delta\theta/2) \approx \delta T\,\delta\theta \approx \delta p(r\delta\theta) \implies \delta T = r\delta p. \tag{1.9}$$

$$\therefore \quad \delta T = Eh\frac{\delta \ell}{\ell} = Eh\frac{\delta r}{r} \quad (\Longleftarrow \ell = r\delta\theta)$$

$$= \frac{Eh}{2}\frac{\delta A}{A} \quad \text{since} \quad \left(A = \pi r^2 \implies \frac{\delta A}{A} = \frac{2\pi r \delta r}{\pi r^2} = \frac{2\delta r}{r}\right). \tag{1.10}$$

From Eqs. (1.6) and (1.7),

$$c_0^2 = \frac{A_0 P'(A_0)}{\rho} = \frac{A_0}{\rho}\frac{\delta p}{\delta A}$$

and, using Eqs. (1.9) and (1.10), we see that

$$c_0^2 = Eh/2\rho r_0, \tag{1.11}$$

where r_0 is the mean radius of the tube. This is the Moens-Korteweg wave speed (1878), although first discovered by Young in (1809).

c_0 as calculated from Eq. (1.11) is quite accurate predicting that $c_0 \approx 5\,\text{ms}^{-1}$ in the human thoracic aorta and increases to about $8\,\text{ms}^{-1}$ in the large peripheral arteries. However, refinements of the elastic theory to include longitudinal stresses and dynamic elastic properties increase c_0 by about 25% worsening the agreement with experiments.

Also Eq. (1.8) predict that the velocity and pressure wave forms will be the same and propagate without change of shape, in contradiction to the following observations, so other effects need to be included.

1.2.5. Observations.

1. Velocity wave form different from pressure wave form
   - use viscous fluid theory in a rigid tube and can successfully predict velocity wave form from pressure wave form.
2. Peaking of pressure wave
   - explained by reflections.
3. Attenuation (experiments at high frequency)
   - need viscoelastic effects to model successfully, viscous fluid is insufficient.

1.3. Wave reflections

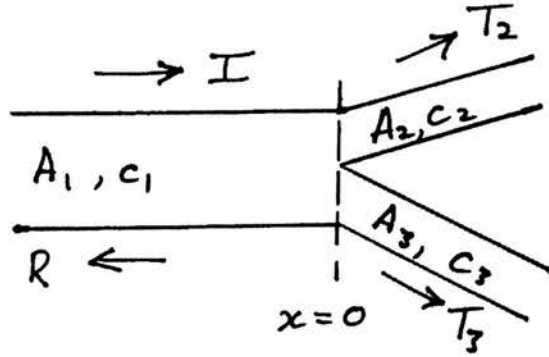The aim is to explain the peaking of the pressure pulse (see Fig. 8).

FIGURE 8. Wave reflection at a bifurcation. I – incident wave, R – reflected wave,
T – transmitted wave, A – cross-sectional area, c – wave-speed.

We begin by analysing the reflection and transmission of a wave at an isolated bifurcation. The incident pressure wave is $p_I = P_I f(t - x/c_1)$. P_I is the amplitude, f is the wave form. The flow rate associated with the incident wave is $A_1 u_I$ which equals

$$Q_I = Y_1 P_I f(t - x/c_1),$$

where $Y_1 = A_1/\rho c_1$ from (1.8), is the characteristic admittance. (Here A_1 is the undisturbed area and we have neglected the perturbation, a.)

The reflected wave has pressure

$$p_R = P_R \, g(t + x/c_1)$$

and flow

$$Q_R = -Y_1 P_R \, g(t + x/c_1)$$

and, for the transmitted waves,

$$p_j = P_j h_j(t - x/c_j), \quad Q_j = Y_j P_j h_j(t - x/c_j),$$

where

$$Y_j = A_j/\rho c_j \quad (j = 2, 3).$$

We need to match the pressure and the flow rate at the bifurcation at all times at $x = 0$, thus

$$\implies g(t) = h_j(t) = f(t),$$

$$P_{\mathrm{I}} + P_{\mathrm{R}} = P_2 = P_3 \quad \text{and} \quad Y_1(P_{\mathrm{I}} - P_{\mathrm{R}}) = Y_2 P_2 + Y_3 P_3 \tag{1.12}$$

$$\implies \frac{P_{\mathrm{R}}}{P_{\mathrm{I}}} = \frac{Y_1 - (Y_2 + Y_3)}{Y_1 + (Y_2 + Y_3)}$$

and

$$\frac{P_2}{P_{\mathrm{I}}} = \frac{P_3}{P_{\mathrm{I}}} = \frac{2Y_1}{Y_1 + (Y_2 + Y_3)}. \tag{1.13}$$

Notes:

1. If $Y_2 + Y_3 < Y_1$, then the reflected pressure wave is in phase with the incident wave at $x = 0$ and the combined amplitude $P_{\mathrm{I}} + P_{\mathrm{R}}$ is greater than P_{I} alone. This is a "closed end" type of junction.

2. If $Y_2 + Y_3 > Y_1$, P_{R} is of opposite phase and the combined amplitude $P_{\mathrm{I}} - P_{\mathrm{R}}$ is less than P_{I} alone. This is an "open end" junction.

3. If $Y_2 + Y_3 = Y_1$, $P_{\mathrm{R}} = 0$, there is no reflection and the junction is well-matched.

4. Most cardio-vascular junctions are well-matched except, notably in man, the iliac bifurcation which is of the closed-end type. This is certainly a contributing factor to the peaking of the pressure pulse, although taper is also important.

1.4. Effect of viscosity – Womersley's problem

We examine the effect of viscosity on a flow driven by an oscillatory pressure gradient in a rigid tube. The assumption of a rigid tube is satisfactory
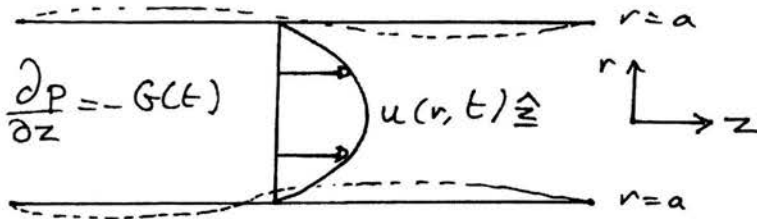

FIGURE 9. Wormersley's problem.

because the distance travelled by a fluid element in 1 cycle $\ll$ wavelength and thus the tube is approximately parallel-sided (see Fig. 9).

The pressure gradient is given as a Fourier expansion in t:

$$\frac{\partial p}{\partial z} = -\Re \left\{ \sum_{n=0}^{\infty} G_n e^{in\omega t} \right\}. \tag{1.14}$$

$4 - 6$ modes are usually sufficient to model the pressure pulse and about 10 modes suffice for the velocity wave form.

The z-component for the Navier–Stokes equations in cylindrical polar coordinates gives

$$u_t = -\frac{p_z}{\rho} + \frac{\mu}{\rho} \left(u_{rr} + \frac{1}{r} u_r \right), \tag{1.15}$$

with b.c.'s $\begin{cases} u = 0 & \text{on} \quad r = a, \\ u_r = 0 & \text{on} \quad r = 0. \end{cases}$ \hfill (1.16)

Suppose that the Fourier series for $u(r, t)$ is

$$u = u_0(r) + \sum_{n=1}^{\infty} u_n(r) e^{in\omega t}. \tag{1.17}$$

Substitute into Eq. (1.15) and solve the linear ODE's term by term. The fundamental mean flow is

$$u_0(r) = \frac{G_0 a^2}{4\mu} \left(1 - \frac{r^2}{a^2} \right) \quad - \quad \text{Poiseuille flow.} \tag{1.18}$$

The oscillatory terms come from solutions of Bessel's Equation (*Exercise*):

$$u_n(r) = \frac{G_n a^2}{i\mu \alpha_n^2} \left[1 - \frac{J_0 \left(i^{3/2} \alpha_n r/a \right)}{J_0 \left(i^{3/2} \alpha_n \right)} \right] \quad (n \geq 1), \tag{1.19}$$

where

$$\alpha_n^2 = \rho n \omega a^2 / \mu, \tag{1.20}$$

$$\alpha^2 = \rho \omega a^2 / \mu \; (\equiv \alpha_1), \tag{1.21}$$

is the Womersley parameter.

For details of Bessel functions, see e.g. I.N. Sneddon, "Special Functions of Mathematical Physics and Chemistry", 3rd edition, Longman, pp. 130–132, which gives

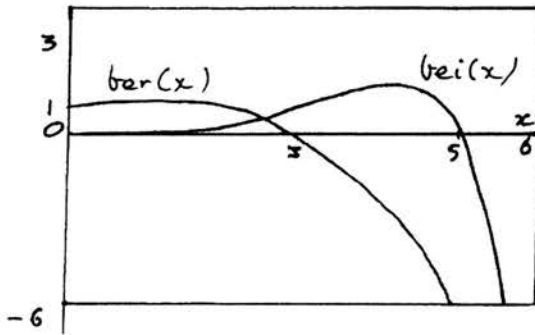$$J_0(i^{3/2}x) = I_0(i^{1/2}x) = \text{ber}\,(x) + i\,\text{bei}\,(x).$$

FIGURE 10. Sketch of the Kelvin functions.

Ber and bei are known as Kelvin (or Thompson) functions (see Fig. 10).

$$\text{ber}(x) = \sum_{s=0}^{\infty}(-1)^s(x/2)^{4s}/(2s!)^2, \quad \text{bei}(x) = \sum_{s=0}^{\infty}(-1)^s(x/2)^{4s+2}/(2s+1)!^2.$$

What does the Womersley parameter measure?

(i) $\alpha^2 = O\left(\left[\dfrac{\partial u}{\partial t}\right] \Big/ \left[\nu\dfrac{\partial^2 u}{\partial r^2}\right]\right)$ = an unsteady Reynolds number.

(ii) $\alpha^2 = (a^2/\nu)\,/\,(1/\omega) \propto \dfrac{\text{viscous diffusion time}}{\text{period}}$ = frequency parameter.

For fluids of small viscosity, so that $\alpha_n \gg 1$, Eqs. (1.17) - (1.20) show that

$$u \sim \frac{G_0}{4\mu}(a^2 - r^2) + \frac{a^2}{\mu}\sum_{n=1}^{\infty}\frac{G_n}{\alpha_n^2}\sin n\omega t$$

$$- \frac{a^2}{\mu}\left(\frac{a}{r}\right)^{1/2}\sum_{n=1}^{\infty}\frac{G_n}{\alpha_n^2}e^{-\alpha_n(1-r/a)/\sqrt{2}}\sin\left[n\omega t - \alpha_n(1-r/a)/\sqrt{2}\right],$$

using the asymptotic behaviour of J_0.

This shows that when $\alpha_n \gg 1$, the flow consists of Poiseuille flow upon which is superimposed an unsteady core flow surrounded by a boundary layer of thickness $0(\alpha_n^{-1})$.

(iii) $\alpha = \dfrac{a}{\sqrt{\nu/\omega}} = \dfrac{\text{radius}}{\text{stokes b.l. thickness}}$ (Exercise).

If α is small, then taking the limits of the Bessel's functions, we find that $|u_n| \ll 1$ for $n \geq 1$ and the u_0 – terms give quasi-steady Poiseuille flow. Interpretation (iii) shows that the boundary layers fill the tube.

If α is large, then (iii) shows that the boundary layers are thin and (ii) shows that vorticity ($\boldsymbol{\omega} = \boldsymbol{\nabla} \cdot \mathbf{u}$) does not have time to diffuse across the tube before the flow reverses.

Experiments in which the pressure gradient waveform and the flow rate $Q(t)$ were measured, show that this theory is successful in explaining the differences between the waveforms.

The flow rate $Q(t) = \int_0^a u(r)\, 2\pi r\, dr$ and using Eq. (1.19)

$$Q(t) = \pi a^2 \left\{ \frac{G_0 a^2}{8\mu} + \frac{a^2}{i\mu} \sum_1^\infty \frac{G_n}{\alpha_n^2} \left[1 - F(\alpha_n)\right] e^{in\omega t} \right\}, \qquad (1.22)$$

where

$$F(\alpha_n) = 2J_1(i^{3/2}\alpha_n)/i^{3/2}\alpha J_0(i^{3/2}\alpha_n),$$

$$\longrightarrow \begin{cases} 1 - \dfrac{i\alpha^2}{8} & \text{as} \quad \alpha \longrightarrow 0 \quad (\text{good for } \alpha < 4), \\[2mm] \dfrac{2}{i^{1/2}\alpha}(1 + \dfrac{1}{2\alpha}) & \text{as} \quad \alpha \longrightarrow \infty \quad (\text{good for } \alpha > 4). \end{cases} \qquad (1.23)$$

1.5. Nonlinear theory

The governing Eqs. (1.1) - (1.3) are hyperbolic so we expect to be able to use the ideas of Riemann invariants, characteristics and shock waves.

We begin by rewriting Eqs. (1.1) - (1.3) as

$$A_t + Au_x + uA_x = 0 \qquad (1.24)$$

and

$$u_t + uu_x + \left(c^2/A\right) A_x = 0, \qquad (1.25)$$

where

$$c^2(A) = AP'(A)/\rho, \qquad (1.26)$$

which is not constant. Adding $\pm c/A$ times (1.24) to (1.25) gives

$$\left(\frac{\partial}{\partial t} + (u \pm c)\frac{\partial}{\partial x}\right)\left[u \pm \int_{A_0}^A \frac{c}{A^*}\, dA^*\right] = 0. \qquad (1.27)$$

$$\left(\text{Note that} \quad \frac{\partial}{\partial t}\int_{A_0}^{A(x,t)} g(A^*)\, dA^* = g(A)\frac{\partial A}{\partial t}\text{etc.}\right)$$

Compare $\partial_t + (u \pm c)\partial_c$ with $D/Dt \equiv \partial_t + u\partial_x$ in 1-D fluid dynamics: if $(\partial_t + u\partial_x)f = 0$, it means that the rate of change of f for a fluid particle moving with speed u is zero.

Thus, from Eq. (1.27) we have that the Riemann invariants

$$R_\pm = u \pm \int_{A_0}^A \frac{c}{A^*} \, dA^*, \tag{1.28}$$

are constant on the characteristics, $C_\pm$, given by

$$C_\pm : \frac{dx}{dt} = u \pm c \tag{1.29}$$

and so nonlinear waves propagate in the $\pm$ x-direction with variable speeds, $u \pm c$.

1.5.1. Shock formation. Propagation speeds are not uniform in general so characteristics can run together and form discontinuities or shocks.

Consider the situation in Fig. 11 where blood is ejected from the left ventricle with velocity

$$U(t) \begin{cases} \geq 0 \text{ at } x = 0 & \text{for } t \geq 0, \\ = 0 \text{ at } x = 0 & \text{for } t < 0. \end{cases}$$
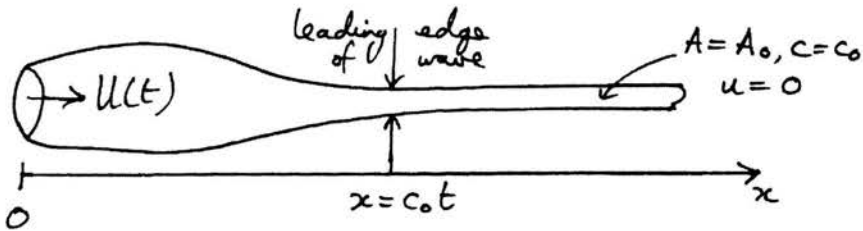

FIGURE 11. Pulse wave moving into undisturbed fluid.

The front of the pulse wave is moving into undisturbed fluid for which $c = c_0$ and so it propagates with speed c_0 (unless a shock forms at the front). This implies that

$$A = A_0, \quad c = c_0 \quad \text{and} \quad u = 0 \quad \text{for} \quad x > c_0 t.$$

Define

$$V(c) \equiv \int_{A_0}^A \frac{c(A^*)}{A^*} \, dA^*, \text{ then } V(c_0) = 0 \quad (\Longleftarrow A = A_0 \text{ when } c = c_0).$$

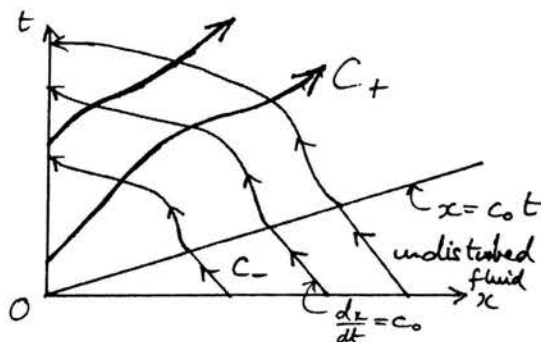We can draw an (x, t) phase diagram (Fig. 12) to show the characteristics.

FIGURE 12. The characteristics for the propagation of the pulse wave.

We know that $R_\pm = $ constant on $dx/dt = u \pm c$.
In $x > c_0 t$, $u = 0$, $c = c_0$ and

$$R_- = 0 \quad \implies \quad u = V(c),$$

on all C_- characteristics originating in $x > c_0 t$, even when they move into the disturbed region.

$$\therefore \quad \underline{u = V(c),} \quad \text{throughout the fluid.}$$

Consider the C_+ characteristics in $x < c_0 t$.

$$u = V(c) \text{ everywhere} \implies R_+ \equiv u + V(c) = 2u$$
$$\implies u = \text{constant everywhere}$$
$$\implies c = \text{constant everywhere}$$
$$(\because \quad u = V(c)) \implies \underline{C_+ \text{ characteristics are straight lines,}}$$

although they can have different slopes.

Shocks form where the characteristics intersect and we can calculate when this will first happen (Fig. 13).

A typical C_+ characteristic starting at $t = \tau$ from $x = 0$ is

$$x = [U(\tau) + c(U(\tau)] (t - \tau), \tag{1.30}$$

with neighbouring characteristic

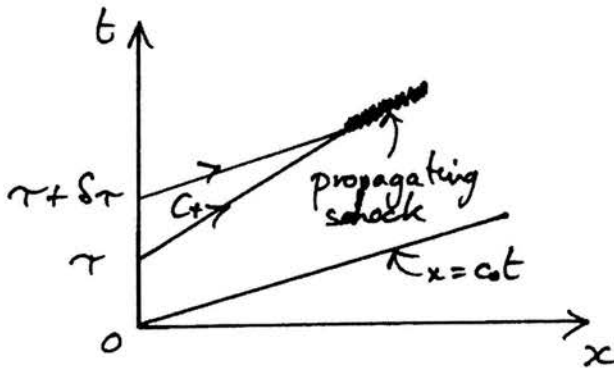$$x = [U(\tau + \delta\tau) + c(U(\tau + \delta\tau))] (t - \tau - \delta\tau). \tag{1.31}$$

FIGURE 13. Shock formation.

Equations (1.30) and (1.31) and letting $\delta\tau \longrightarrow 0$ tells us that the characteristics meet at time

$$t_s = \tau + F(U(\tau))/\dot{u}(\tau)F'(U(\tau)), \tag{1.32}$$

where

$$F(U(\tau)) \equiv U(\tau) + c(U(\tau)). \tag{1.33}$$

A shock will first form when $t_s(\tau)$ has a minimum.

Example

Take $P(A) = \rho c_0^2 A^2/2A_0^2 + \text{constant}$

and $U(t) = \begin{cases} U_0 \left[1 - (1 - t/t_0)^2\right] & 0 \le t \le 2t_0, \\ 0 & t < 0 \text{ and } t > 2t_0. \end{cases}$

(see Fig. 14).

Then $c = c_0 A/A_0$, $V(c) = c_0(A - A_0)/A_0 = c - c_0$ and therefore $F = 2U + c_0$.

Equation (1.32) gives

$$t_s(\tau) = \tau + (c_0 + 2U)\, t_0^2/4U_0(t_0 - \tau)$$

which has a minimum at $\tau = 0$, so that the first shock appears when

$$t_s = c_0 t_0/4U_0 \quad \text{at} \quad x_s = c_0^2 t_0/4U_0.$$

For typical physiological conditions in man, x_s is longer than the aorta and a shock would not be expected to form. However, when there is "aortic
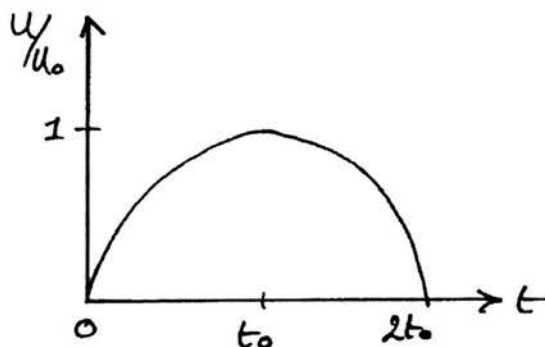
FIGURE 14. Ejection velocity.

valve incompetence", the heart compensates by ejected a greater volume of blood and clinicians report a "pistol-shot pulse", which is likely to correspond to the formation of a shock.

2. Spermatozoa and micro-organisms

Many microscopic creatures, including bacteria and algae, are very active swimmers and have a great variety of sensing mechanisms to find the optimum place to be in their environment. However because they are so tiny, the fluids in which they move (typically water) appear to them to be extremely viscous. Mathematically, the Reynolds number is very small, i.e.

$$R = UL/\nu \ll 1$$

and, taking $R = 0$, the Navier–Stokes equations reduce to

$$0 = -\boldsymbol{\nabla} p + \mu \nabla^2 \mathbf{u}, \tag{2.1}$$

$$\boldsymbol{\nabla} \mathbf{u} = 0, \tag{2.2}$$

plus b.c.'s. These are the slow flow or Stokes Equations. We see that the inertial terms

$$\rho \frac{D\mathbf{u}}{Dt} = \rho \frac{\partial \mathbf{u}}{\partial t} + (\mathbf{u}.\boldsymbol{\nabla}) \mathbf{u},$$

have been neglected so that

  (i) the Stokes equations are <u>linear</u> and we can use superposition of solutions, and

 (ii) time enters the equations only through the motion of the boundaries, i.e. it behaves as a parameter.

As an immediate consequence of linearity (i), it is straightforward to prove that for any given b.c.'s, the solution of the Stokes equations is <u>unique</u>, unlike the full Navier–Stokes equations (up to a constant added to p).

<u>Reversibility</u>

Consider $\nabla p = \mu \nabla^2 \mathbf{u}$, $\nabla.\mathbf{u} = 0$ with b.c.'s $\mathbf{u} = \mathbf{u}_B(\mathbf{x})$ on a boundary S.

Let $p = p_1(\mathbf{x})$, $\mathbf{u} = \mathbf{u}_1(\mathbf{x})$ be the unique solution.

Now reverse the b.c.'s, i.e. set $\mathbf{u} = -\mathbf{u}_B(\mathbf{x})$ on S.

The unique solution is

$$\mathbf{u} = \mathbf{u}_2(\mathbf{x}) = -\mathbf{u}_1(\mathbf{x}), \quad p = p_2(\mathbf{x}) = -p_1(\mathbf{x}).$$

This has an important interpretation: reversed boundary conditions lead to reversed flow.

Consider a mechanical fish which moves according to the Stokes Equations and flaps its tail up and down as shown in Fig. 15.

When the tail flaps downwards, the "fish" may make a little forwards progess but, because the flow is exactly reversed when the tail flaps upwards, it will return to its starting position. Thus a swimming motion which may work well at high Reynolds numbers will not work at all at low Reynolds numbers!

The solution is to use a motion that is irreversible e.g. Figs. 16 and 17.

2.1. The swimming of a thin, flexible sheet

(G.I. Taylor, Proc. Roy. Soc. Lond., A209, pp.447–461, 1951)

This model illustrates the basic ideas in low R swimming and can be applied to ciliated micro-organisms (Fig. 18).

We shall consider the flow in the fluid above the sheet shown in Fig. 19. The coordinates of the particles on the sheet are

$$x_s = x, \quad y_s = a \sin (kx - \omega t). \tag{2.3}$$

The particles move in the y-direction only with speed
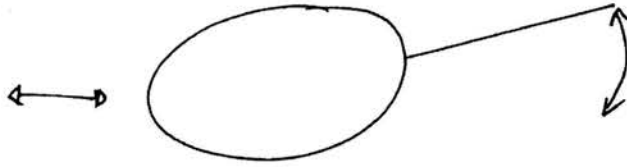
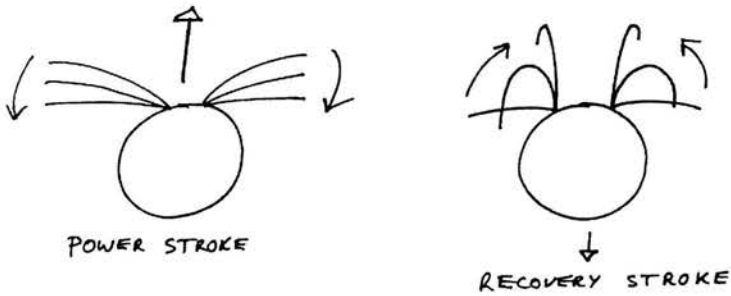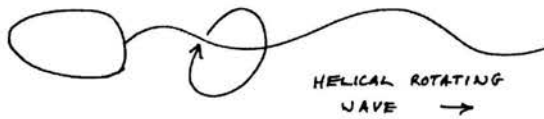$$dy_s/dt = -\omega a \cos (kx - \omega t) \tag{2.4}$$

FIGURE 15. A mechanical fish.

POWER STROKE

RECOVERY STROKE

FIGURE 16. Two steps forward and one step back as used by the alga *Chlamydomonas nivalis*: left-power stroke, right-recovery stroke.

HELICAL ROTATING WAVE →

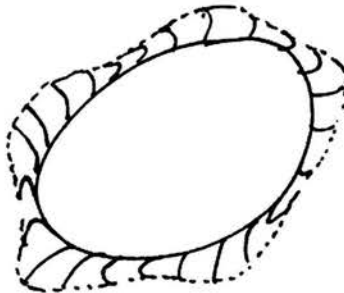FIGURE 17. A sperm or a bacterium passes a helical, rotating wave along the tail.
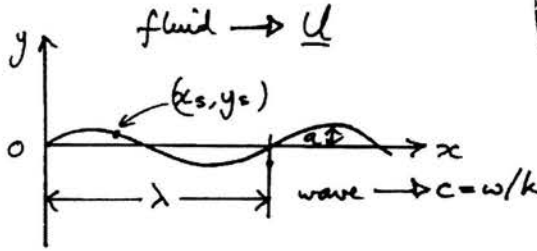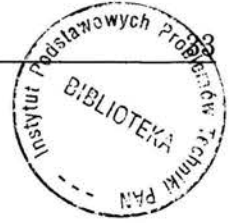

FIGURE 18. A typical ciliated micro-organism.

FIGURE 19. A swimming sheet.

and a wave travels along the sheet in the positive x-direction with speed

$$c = \omega/k. \tag{2.5}$$

Notice that as the particles move up and down, the spacing between them varies so that the sheet stretches and is extensible. A model for a flexible membrane would need to be modified so that it would be inextensible.

The motion is irreversible; reversing the b.c's reverses the direction of propagation of the wave.

We shall show that the oscillations of the sheet induce not only an oscillatory flow but a steady flow component

$$U\mathbf{i} = 2\pi^2 \left(a/\lambda\right)^2 c\mathbf{i},$$

where $\lambda = 2\pi/k$ is the wavelength in the case when $a \ll \lambda$. Equivalently, if the fluid far away from the sheet is at rest, then the sheet moves to the left with speed U.

We can automatically satisfy incompressibility in this 2D model by using a stream function $\psi(x, y)$ defined by

$$u = \partial\psi/\partial y, \quad v = -\partial\psi/\partial x. \tag{2.6}$$

The lines $\psi = $ constant are the streamlines for the flow, since on streamlines

$$\frac{dx}{u} = \frac{dy}{v} \Longleftrightarrow u\,dy - v\,dx = 0$$

$$\Longleftrightarrow \quad d\psi \equiv \frac{\partial\psi}{\partial x}dx + \frac{\partial\psi}{\partial y}dy = 0 \quad \Longleftrightarrow \quad \psi = \text{constant}.$$

$$\text{Check:} \quad \boldsymbol{\nabla}.\mathbf{u} \equiv \frac{\partial u}{\partial x} + \frac{\partial v}{\partial y} \equiv \frac{\partial^2\psi}{\partial x\partial y} - \frac{\partial^2\psi}{\partial y\partial x} \equiv 0,$$

so Eq. (2.2) is satisfied.

2.1.1. Governing equation. Equation (2.1) implies that

$$\frac{\partial p}{\partial x} = \mu \nabla^2 \frac{\partial \psi}{\partial y}, \tag{2.7}$$

$$\frac{\partial p}{\partial y} = -\mu \nabla^2 \frac{\partial \psi}{\partial x}. \tag{2.8}$$

Taking $\partial/\partial y$ (2.8) - $\partial/\partial x$ (2.9) gives

$$\nabla^4 \psi \equiv \left(\frac{\partial^2}{\partial x^2} + \frac{\partial^2}{\partial y^2} \right)^2 \psi = 0, \tag{2.9}$$

- the biharmonic equation.

2.1.2. Boundary conditions. This needs to be solved for ψ subject to suitable b.c.'s as $y \longrightarrow \infty$ ($|\mathbf{u}| < \infty$) and on the sheet (x_s, y_s).

On the sheet, $u_s = 0, \quad v_s = -\omega a \cos(kx - \omega t)$ (from Eq. (2.4))

$$\implies \left. \begin{array}{rcl} \frac{\partial \psi}{\partial y} &=& 0 \\[4pt] \frac{\partial \psi}{\partial x} &=& +\omega a \cos(kx - \omega t) \end{array} \right\} \quad \text{on} \quad y = a\sin(kx - \omega t). \tag{2.10}$$

Note that t only appears in the b.c.'s and is a parameter, and so we can solve the problem at $t = 0$ and calculate the flow at any other time by replacing kx in our solution by $(kx - \omega t)$.

2.1.3. Scaling. Define $x' = kx, \quad y' = ky, \quad \psi' = k\psi/\omega a$ and drop the primes to get

$$\nabla^4 \psi = 0, \tag{2.11}$$

$$\partial \psi/\partial y = 0, \quad \partial \psi/\partial x = \cos x \quad \text{on} \quad y = \epsilon \sin x, \tag{2.12}$$

$$\text{where} \quad \epsilon = ka = 2\pi a/\lambda. \tag{2.13}$$

The flexing of the boundary ($\Longleftarrow y = \epsilon \sin x$) makes it difficult to find an exact solution. Instead we shall assume that $\epsilon \ll 1$ and expand the b.c.'s Eq. (2.12) in a Taylor Series about $y = 0$:

$$\begin{array}{rcl} \psi_y \mid_{y=0} + \epsilon \sin(x)\psi_{yy} \mid_{y=0} + \dots &=& 0, \\[4pt] \psi_x \mid_{y=0} + \epsilon \sin(x)\psi_{yx} \mid_{y=0} + \dots &=& \cos(x). \end{array} \tag{2.14}$$

We seek a solution in powers of ϵ:

$$\psi = \psi_0 + \epsilon \psi_1 + \epsilon^2 \psi_2 + \dots, \tag{2.15}$$

Substituting Eq. (2.15) into the governing Eq. (2.11) and the b.c's Eq. (2.12), and equating coefficients of successive power of t to zero, we obtain at O(1)

$$\nabla^4\psi_0 = 0; \quad \psi_{0y} = 0, \quad \psi_{0x} = \cos x \quad \text{on} \quad y = 0 \qquad (2.16)$$

and at $O(\epsilon)$

$$\nabla^4\psi_1 = 0; \quad \begin{aligned} \psi_{1y} + \psi_{0yy}\sin x &= 0, \\ \psi_{1x} + \psi_{0yx}\sin x &= 0 \quad \text{on} \quad y = 0, \end{aligned} \qquad (2.17)$$

etc. The general solutions of the O(1) problem with the correct x-dependence are

$$\psi_0 = \left[(A + By)e^{-y} + (C + Dy)e^{+y}\right]\sin x.$$

(Check by substitution)
For u and v to be bounded as $y \longrightarrow \infty$, we need $C = D = 0$.

To satisfy the b.c.'s in Eq. (2.16), we need $A = B = 1$ so that

$$\psi_0 = (1 + y)e^{-y}\sin x. \qquad (2.18)$$

Substituting (2.18) into the b.c's in (2.17), we get

$$\psi_{1y} = \sin^2 x, \quad \psi_{1x} = 0 \quad \text{on} \quad y = 0. \qquad (2.19)$$

On writing $\sin^2 x = (1 - \cos 2x)/2$, we seek solutions like

$$\psi_1 = f(y) + g(y)\cos 2x$$

and after substituting into the biharmonic equation find that

$$\psi_1 = \left[(E + Fy)e^{-2y} + (G + Hy)e^{+2y}\right]\cos 2x + \left[Ay^3 + By^2 + Cy + D\right].$$

For u, v to be bounded as $y \longrightarrow \infty$, we need $G = H = A = B = 0$ and then, on satisfying the boundary conditions (2.19), we arrive at

$$\psi_1 = \frac{y}{2} - \frac{y}{2}e^{-2y}\cos 2x. \qquad (2.20)$$

Combining these results, (2.18) and (2.20) and differentiating gives

$$u \equiv \frac{\partial\psi}{\partial y} = -ye^{-y}\sin x + \epsilon\left[\frac{1}{2} + \left(y - \frac{1}{2}\right)e^{-2y}\cos 2x\right] + \dots. \qquad (2.21)$$

Returning to the dimensional variables and incorporating the parameter t finally yields for the horizontal component of velocity

$$u = -\epsilon \omega y e^{-ky} \sin(kx - \omega t)$$
$$+ \underbrace{\epsilon^2 c [1/2}_{\text{steady term}} + \left(ky - \tfrac{1}{2}\right) e^{-2ky} \cos 2(kx - \omega t)] + \ldots, \qquad (2.22)$$

which has a steady term $U = \epsilon^2 c / 2$.

We conclude that the sheet can indeed swim with speed proportional to amplitude squared and the wave speed c.

2.2. Resistive force theory for flagellar propulsion

(Gray & Hancock, Journal of Experimental Biology, **32**, 802–14, 1955.)

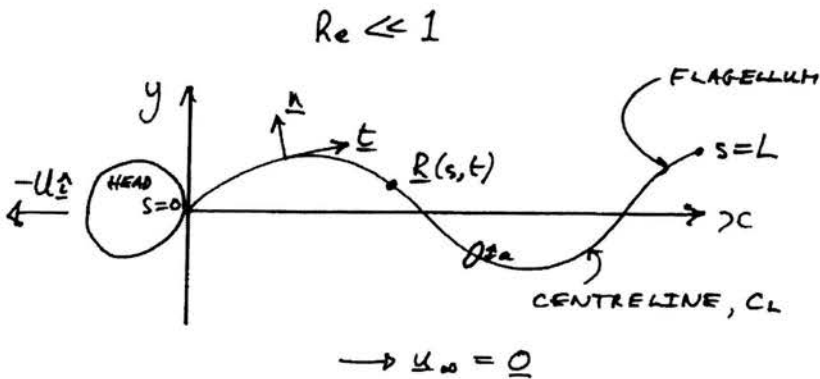Consider a flagellated micro-organisms such as a spermatazoon (Fig. 20).

FIGURE 20. A flagellated micro-organism.

A wave of bending (planar or helical) is passed backwards along C_{L}. The wave is of uniform amplitude and the flagellum is inextensible. At any instant, the position of a material point on C_{L} is

$$\mathbf{r} = \mathbf{R}(s) = [X(s), Y(s), Z(s)], \qquad (2.23)$$

where

$$X(s + \Lambda) = X(s) + \lambda, \quad Y(s + \Lambda) = Y(s), \quad Z(s + \Lambda) = Z(s). \qquad (2.24)$$

This is different to the sheet because it is not of infinite width, can deal with helical waves, only requires a small slope rather than amplitude and is of finite length, but it approximates the fluid mechanics.

Let Λ be wavelength along C_L; λ is its projection on to x-axis.

The mean velocity of whole organism relative to fluid at rest at ∞ is $-U\mathbf{i}$.

Assume that $a \ll d \ll \lambda < \Lambda$, $d \ll L$. L is the total length of the flagellum and

$$\alpha \equiv \lambda/\Lambda < 1. \tag{2.25}$$

2.2.1. Kinematics. We need to know velocity of material points on the flagellum relative to fluid at rest at ∞ and to apply the condition of inextensibility (see Fig. 21).
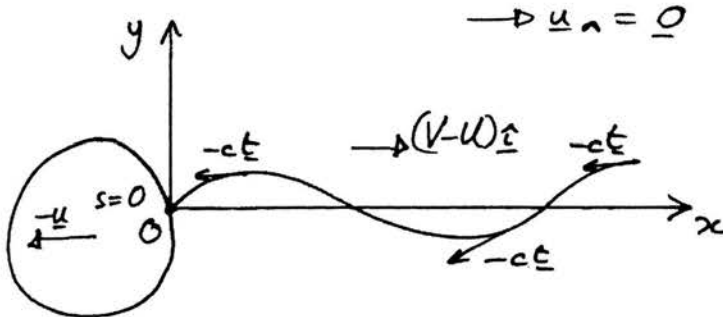

FIGURE 21. Velocity of material points on the flagellum.

Suppose that a wave propagates in the x-direction with speed $V\mathbf{i}$ relative to the mean speed, $U\mathbf{i}$, of the organism $(V > U)$.

A reference frame moving with speed $(V - U)\mathbf{i}$ relative to fluid at ∞ moves with the crests (and troughs) of the waves.

Material points appear to move through the crests with speed

$$c = V(\Lambda/\lambda) = V/\alpha \quad \Longleftrightarrow \quad V = \alpha c, \tag{2.26}$$

since over one wavelength, the arclength $= \Lambda$ and the its projection onto the x-axis $= \lambda$.

The flagellum is inextensible $\Longrightarrow$ all material points move with the same speed (but in different directions) tangentially, so the velocity relative to

crests is $-c\mathbf{t}$, where $\mathbf{t}$ is the tangent to surface. The velocity of material points relative to the fluid at ∞ is

$$(V - U)\mathbf{i} - c\mathbf{t} \equiv -\mathbf{w}. \tag{2.27}$$

2.2.2. Resistive force theory. This theory treats each part of the flagellum locally as being part of a long cylinder. Since the Stokes equations are <u>linear</u>, the normal and tangential components of the drag force on any body are proportional to its normal and tangential components of velocity relative to the fluid velocity, respectively. For a long cylinder these components can be calculated.

For an element ds of the flagellum (Fig. 22), the element of force exerted by the fluid is

$$d\mathbf{F} = [K_t\,(\mathbf{w.t})\,\mathbf{t} + K_n\,(\mathbf{w.n})\,\mathbf{n}]\,ds. \tag{2.28}$$

K_t and K_n are the tangential and normal resistance coefficients for a thin cylinder of unit length.
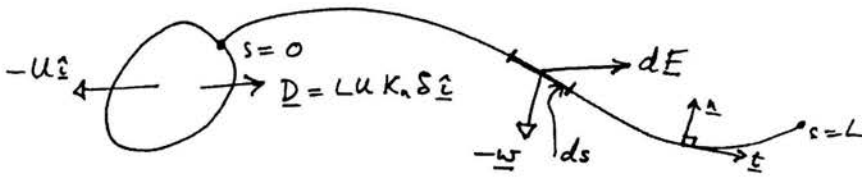

FIGURE 22. Forces on an element of the flagellum. Note the sign of $d\mathbf{F}$.

The total force on the flagellum in the $\mathbf{i}$ – direction is minus the thrust, T, and thus

$$-T = \int_{s=0}^{L} d\mathbf{F} \cdot \mathbf{i} = (K_t - K_n) \int_0^L (\mathbf{w.t})\,(\mathbf{t.i})\,ds + K_n \int_0^L (\mathbf{w.i})\,ds, \tag{2.29}$$

$$(\Longleftarrow \mathbf{w.i} = (\mathbf{w.n})\,(\mathbf{n.i}) + (\mathbf{w.t})\,(\mathbf{t.i}))\,.$$

By definition, $\mathbf{t} = d\mathbf{R}/ds \Longrightarrow \mathbf{t.i} = X'(s)$. From (2.27),

$$\mathbf{w.t} = (U - V)\,\mathbf{i.t} + c,$$
$$\mathbf{w.i} = U - V + c\,\mathbf{i.t}.$$

Hence

$$-T = (K_t - K_n)\,(U - V) \int_0^L X'^2\,ds + K_n\,(U - V)\,L + K_t c \int_0^L X'\,ds. \tag{2.30}$$

Now $\int_0^L X' \, ds = \alpha L = VL/c$ and we write $\int_0^L X'^2 ds = \beta L$, where $0 < \beta < 1$ (since $|X'| \leq 1$) to obtain

$$+T = (V - U)\left[(K_t - K_n)\beta L + K_n L\right] - K_t V L. \qquad (2.31)$$

This result depends on the resistance coefficients, K_t and K_n, and on β which depends on the waveform and which we have to calculate for each particular case.

Case:

(i) *Zero thrust swimming (no head)*.

$$T = 0 \quad \Longrightarrow \quad U = \frac{V(1 - \beta)(1 - \gamma)}{1 - \beta(1 - \gamma)}, \quad \gamma \equiv K_t/K_n. \qquad (2.32)$$

Thus if $\gamma < 1$ a backwards travelling wave propels the creature forwards. For a smooth cylinder $\gamma \sim 1/2$. Note that only the ratio of the coefficients is important.

However if $\gamma > 1$, then the wave must travel forwards to pull the microorganism forwards. This really happens in nature with polychaete marine worms such as *Nereis* (albeit at moderate values of R) and with some algae such as *Chrysomonad* and the parasites, trypanosomatids, which have "hairy" or mastigoneme flagella (see Fig. 23).
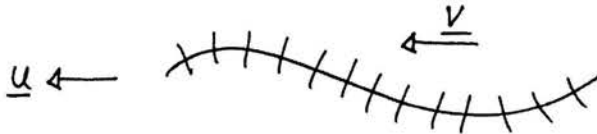

FIGURE 23. A mastigoneme flagellum.

(ii) *The thrust balances the drag on the rest of the body or head*.
   $T = D = LUK_n\delta$, say. (The term LUK_n is just a suitable scaling for D.) From (2.31)

$$U = V(1 - \beta)(1 - \gamma) / [1 + \delta - \beta(1 - \gamma)]. \qquad (2.33)$$

This result can be compared with experiments as Gray and Hancock did for sea urchin spermatazoa. They found good agreement when $\gamma \approx 1/2$.

2.2.3. Inconsistencies in the choice of γ. For a long straight cylinder with length $q \gg$ its radius a, it is possible to solve the Stokes Equations to get

$$K_t \approx 2\pi\mu/\log(q/\epsilon a), \quad K_n = 4\pi\mu/[\log(q/\epsilon a) + 1], \quad \text{where} \quad \epsilon = \sqrt{e}/2$$

$$\Longrightarrow \gamma = \frac{1}{2} + \frac{1}{2\log(q/\epsilon a)}. \tag{2.34}$$

If $\gamma = 1/2 \iff \log(q/\epsilon a) \gg 1 \iff q \gg a$ and in fact $q \geq \lambda$.

This is inconsistent with the assumption that the flagellum is made up of lots of little straight cylinders. The inconsistency arises from neglecting the fluid velocity due to neighbouring cylinders. Nevertheless Lighthill (1976) showed how to produce a rational self-consistent theory based on slender body theory.

2.2.4. Mechanical efficiency. The rate at which work is done by the flagellum is

$$
\begin{aligned}
W_s &= \int_0^L \mathbf{w}.d\mathbf{F} + DU \\
&= \int_0^L \left[(K_t - K_n)(\mathbf{w}.\mathbf{t})^2 + K_n w^2 \right] ds + DU, \quad \text{from (2.30)} \\
\Longrightarrow & \qquad \qquad \qquad \qquad \qquad \qquad \qquad \qquad \qquad \qquad \qquad (2.35) \\
W_s &= K_t L \left[(V - U)^2 \beta - 2(V - U)c\alpha + c^2 \right] \\
&\quad + K_n L (V - U)^2 (1 - \beta) + K_n L U^2 \delta.
\end{aligned}
$$

Define the hydromechanical efficiency as

$\eta =$ (rate of work needed to pull the non-swimming organism in a straight line through the fluid at speed U ($=$ minimum drag))/ (actual rate of working when swimming over with speed U in a straight line). Thus

$$\eta = (K_t + K_n\delta)LU^2/W_s, \tag{2.36}$$

where W_s is given by (2.34).

FIGURE 24. A sawtooth wave.

We can find the most efficient waveform by maximising η with respect to α and β, which gives

$$\eta_{\max} = \left(1 - \sqrt{\gamma}\right)^2 / \left(1 + \delta\right),$$

where

$$U = V\left(1 - \sqrt{\gamma}\right) / \left(1 + \gamma\right)$$

and thus optimum shape is the saw tooth (Fig. 24). For helical waves, we also need to consider torque balances about the x-axis.

3. Red blood cells and capillaries

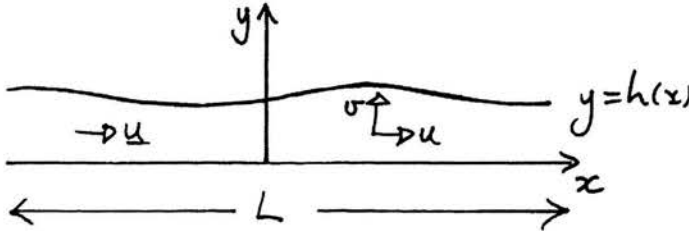### 3.1. Revision of thin film and lubrication theory

FIGURE 25. A lubrication layer.

Consider a typical lubrication layer as illustrated in Fig. 25.
- 2D here but readily extended to 3D.
- Small gap: $h \ll L$.
- Typical fluid speed is U.
- Scaling arguments.

$$\frac{\partial u}{\partial y} \sim \frac{U}{h} \gg \frac{\partial u}{\partial x} \sim \frac{U}{L}$$

$$\implies \quad \nu\nabla^2 \mathbf{u} \approx \nu\frac{\partial^2 \mathbf{u}}{\partial y^2},$$

$$(\mathbf{u}.\boldsymbol{\nabla})\,\mathbf{u} \sim \frac{U^2}{L}\left(1, \frac{h}{L}\right) \quad \text{and} \quad \nu\frac{\partial^2 \mathbf{u}}{\partial y^2} \sim \frac{\nu U}{h^2}\left(1, \frac{h}{L}\right),$$

$$\text{since} \quad \boldsymbol{\nabla}.\mathbf{u} = 0 \quad \implies \quad \frac{\partial u}{\partial x} + \frac{\partial v}{\partial y} = 0 \quad \implies \quad v \sim \frac{Uh}{L}.$$

For the inertial terms to be much smaller than the viscous terms in the Navier–Stokes equations, we need $Uh^2/\nu L \ll 1$.

The Navier–Stokes equations reduce to

$$\therefore \quad \nabla p = \mu \frac{\partial^2 \mathbf{u}}{\partial y^2} \quad \text{and} \quad \nabla.\mathbf{u} = 0. \tag{3.1}$$

$$p_x \sim \mu \frac{U}{h^2}, \quad p_y \sim \frac{\mu}{h^2} \left(\frac{Uh}{L} \right)$$

$$\implies \quad p_y \ll p_x \quad \implies \quad p = p(x) \quad \text{only.}$$

Integrating the x-component of (3.1) with respect to y gives

$$u = \frac{1}{2\mu} \left(\frac{dp}{dx} \right) y^2 + Ay + B,$$

where A, B are constants to be determined from the b.c.'s.

The flux is $q = \displaystyle\int_0^h u(y)\, dy.$

The stress tensor is

$$\sigma = -p\mathsf{I} + 2\mu\mathsf{e}, \quad \mathsf{e} = \frac{1}{2}\left(\nabla \mathbf{u} + (\nabla \mathbf{u})^T \right),$$

$$p \sim \frac{\mu U L}{h^2}, \quad |\mathsf{e}| \sim \frac{\mu U}{h} \ll p.$$

$\therefore \quad \sigma \approx -p\mathsf{I} \quad \implies \quad$ large normal stresses at the boundaries.
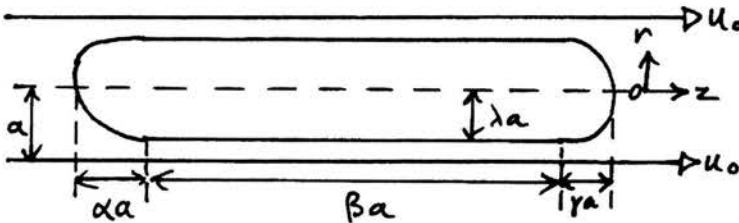

FIGURE 26. A cell squeezing through a very narrow tube.

3.2. Near-critical cell shapes

The flow of a rigid particle through a narrow tube can give insights into the behaviour of a flexible red blood cell at near-minimal diameters.

Consider a cylindrical particle with hemispheriodal ends as shown in Fig. 26. Using lubrication theory in the narrow gap, we get

$$\frac{\mu}{r}\frac{\partial}{\partial r}\left(r\frac{\partial u}{\partial r}\right) = \frac{dp}{dz} \tag{3.2}$$

in the axial direction, with b.c.'s

$$\text{and } \begin{cases} u = 0 & \text{on the particle wall, } r = r^*(z), \\ u = u_0 & \text{on } r = a. \end{cases}$$

Integrating (3.2) and applying the boundary conditions gives

$$\frac{dp}{dz} = g(r^*) \equiv \frac{16\mu}{a^2 - r^{*2}}\frac{\left\{u_0\left[\dfrac{a^2}{2} + \dfrac{a^2 - r^{*2}}{4\ln(r^*/a)}\right] - aq_0\right\}}{\left\{a^2 + r^{*2} + \dfrac{a^2 - r^{*2}}{\ln(r^*/a)}\right\}}, \tag{3.3}$$

where

$$q_0 = \int_{r^*}^{a} u(r, z)\frac{r}{a}\,dr, \tag{3.4}$$

is the "leakback", i.e. the volume flow per unit vessel circumference relative to the cell, which is independent of z.

Integrating with respect to z gives the pressure drop in the limit as $\lambda \longrightarrow 1$,

$$\triangle p = \frac{6\mu u_0}{a}\left\{(\alpha + \gamma)(I_2 - CI_3) + \beta\left[\frac{1}{(1 - \lambda)^2} - \frac{C}{(1 - \lambda)^3}\right]\right\}, \tag{3.5}$$

where $I_n = \displaystyle\int_0^{\pi/2}\frac{\sin\theta}{(1 - \lambda\sin\theta)}\,d\theta$ $(n = 1, 2, 3)$ and $C = 2q_0/au_0$.

(The errors in using (3.2) around the ends of the particle turn out to be small since the pressure gradients are much greater where the gap is narrow).

From (3.3), the shear stress on the cell is

$$\tau(r^*) = \frac{1}{2}g(r^*)\left[\frac{a^2 - r^{*2}}{r^*\ln(r^*/a)} + 2r^*\right] - \frac{\mu u_0}{r^*\ln(r^*/a)}. \tag{3.6}$$

To evaluate q_0 for rigid particles, we use the "zero-drag" condition applied to a cylindrical region of radius a and of length equal to the length of the cell which gives

$$\pi a^2 \triangle p + F = 0,$$

where F is the integral of the wall shear stress, τ_w, over the wall.

To obtain a simpler expression for τ_w, we now assume that the gap width is small compared to a and set $r^* = a(1 - \lambda)$ where $0 < \varepsilon = 1 - \lambda \ll 1$ in (2) to get

$$\tau_w(\lambda) = \left[6\mu q_0/a^2(1 - \lambda)^2\right] - \left[4\mu u_0/a(1 - \lambda)\right]. \tag{3.7}$$

Integrating (3.7) to obtain F gives

$$F = 2\pi a \mu u_0 \left[(\alpha + \gamma)(3CI_2 - 4I_1) + \beta\left(\frac{3C}{(1 - \lambda)^2} - \frac{4}{1 - \lambda}\right)\right].$$

The integrals I_n can be integrated and yield

$$I_1 = \frac{2\lambda^* - \pi/2}{\lambda}, \quad I_2 = \frac{1 + 2\lambda\lambda^*}{1 - \lambda^2}, \quad I_3 = \frac{1 + \lambda^2/2 + 3\lambda\lambda^*}{(1 - \lambda^2)^2},$$

where

$$\lambda^* = \frac{1}{(1 - \lambda^2)^{1/2}} \left[\tan^{-1}\left\{\frac{1 - \lambda}{(1 - \lambda^2)^{1/2}}\right\} + \tan^{-1}\left\{\frac{\lambda}{(1 - \lambda^2)^{1/2}}\right\}\right].$$

Thus $\triangle p$ and q_0 can be calculated for given values of $u_0, \alpha, \beta, \gamma$ and λ.

Numerical studies by D. Halpern & T.W. Secomb, (1989) J. Fluid Mech. 203, pp. 381-400, showed that in very narrow capillaries such as are found in bone marrow, the spleen and partially collapsed or occluded capillaries, red blood cells approach the limits of deformability and their shape is reasonably well approximated by a rigid cell. This occurs for values of a between $1.42\,\mu$m and $1.55\,\mu$m, $1.42\,\mu$m is the minimum radius and when $a > 1.55\,\mu$m the rear of the cell starts to flatten and become concave.

3.3. Red blood cells: single-file flow in narrow capilliaries

Red blood cells (erythrocytes) can adopt a variety of different configurations, as shown in Figs. 27, 28 and 29 (reference: Erythrocyte Mechanics & Blood Flow, 1980, eds. G.R. Cokelet, H.J. Meiselman & D.E. Brooks).

Mamalian erythrocytes are highly deformable – they have to be to travel through capilliaries of $\geq 3\,\mu$m diameter!

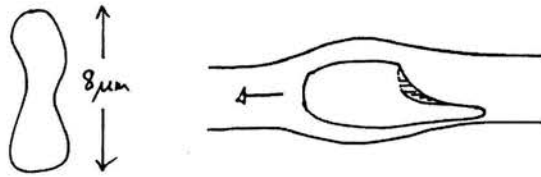Deformability and stirring of contents enhances transport across membrane?
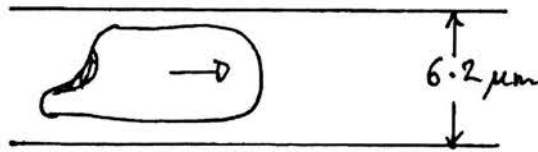
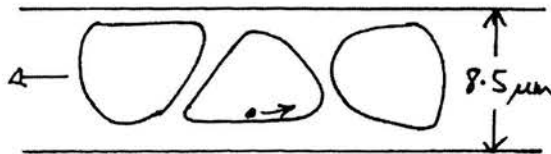FIGURE 27. Erythrocytes.

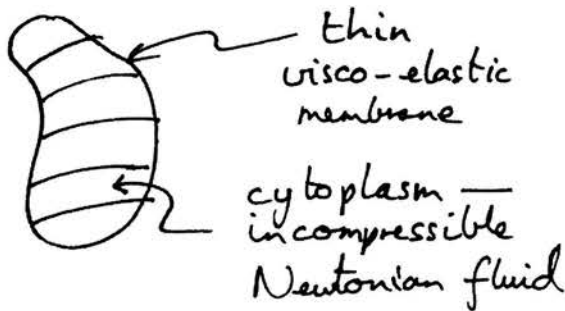FIGURE 28. Slipper shape.

FIGURE 29. Tank treading.

FIGURE 30. Material properties of red blood cells.

3.3.1. Membrane properties. Steady flows so we shall only need to consider the elastic properties.

- Bending modulus $= 1.8 \cdot 10^{-12}\,\mathrm{dyn\,cm^{-1}}$.
- Shear modulus $= 4.2 \cdot 10^{-3}\,\mathrm{dyn\,cm^{-1}}$.
- Dilatation modulus $= 500\,\mathrm{dyn\,cm^{-1}}$.

  ($1\,\mathrm{dyn} = 10^{-5}\,\mathrm{N}$).

There are tension, shear and bending stresses in the membrane. However the bending stresses are very small except at very sharp corners so they can be neglected. On the other hand, it's difficult to build up large shear stresses in the membrane without some dilatation and hence very large isotropic tensions. Therefore we assume that membrane is inextensible and can support tension. The geometry is difficult so we consider a two-dimensional model of an asymmetric cell. (See T.W. Secomb & R. Skalak (1982) Microvascular Research 24, 194–203.)

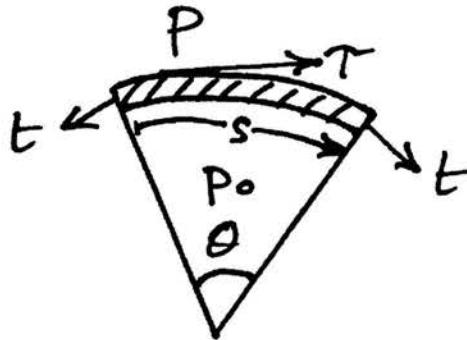**3.3.2. The membrane equations.** Consider the force balance on an element of a cell's membrane (Fig. 31).

FIGURE 31. A tank treading red blood cell.

$$p_0 - p = t\frac{d\theta}{ds} \quad \text{and} \quad \frac{dt}{ds} = -\tau.$$

3.3.3. The 2D model for tank-treading. Consider a tank treading erythrocyte as shown in Fig. 32.

- Reference frame moves with cells.
- Pressure $= p_0$ within cell so that the back is floppy.
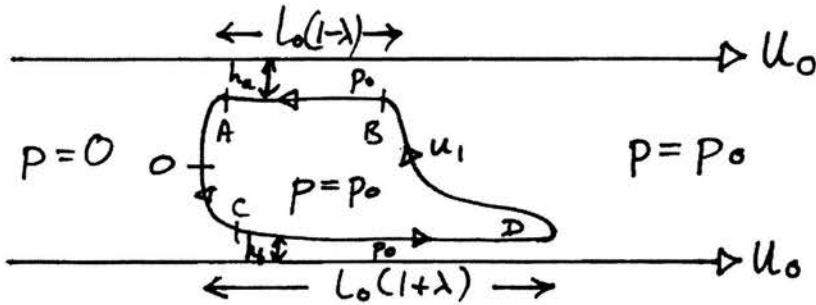- Viscosity of cytoplasm is negligible.

FIGURE 32. A tank treading red blood cell.

- Narrow gaps along AB, $CD \implies$ lubrication theory.
- $p = p_0$ in narrow gaps too, otherwise non-zero tension $\implies$ membrane is curved.
- $p = 0$ at front end $\implies$ constant tension between A and $C \implies$ circularly shaped nose.
- 2-D model with tank-treading and asymmetry.
- Force balance on cell $\implies$ tension falls with distance towards rear. Tension $= 0$ at B and D.
- u_0, λ are given. Seek to determine $p_0, u_1, h_a, h_b, t(0)$.

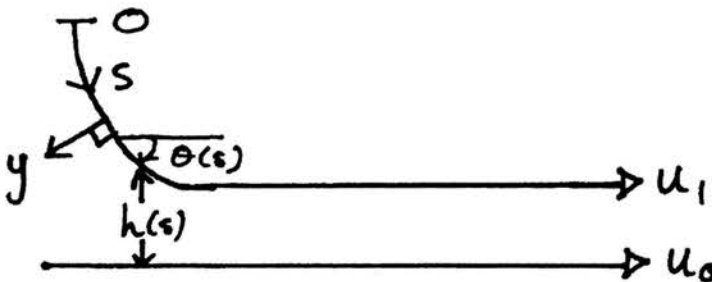**3.3.4. The lower gap OCD.** Use *lubrication theory* in the almost parallel region (Fig. 33).

FIGURE 33. The lower gap in the model of a tank treading red blood cell.

$$\implies \quad p = p(s), \quad \frac{\partial^2 u}{\partial y^2} = \frac{1}{\mu}\frac{dp}{ds},$$

$$\implies \quad u = -\frac{1}{2\mu}\frac{dp}{ds}\,y(h-y) + u_1 + (u_0 - u_1)\frac{y}{h}.$$

In steady flow, the flow rate $q_0 = $ const, where

$$q_0 = \int_0^h u\,dy = \frac{1}{2}(u_0 + u_1)h - \frac{h^3}{12\mu}\frac{dp}{ds}.$$

The *membrane equations* give

$$p_0 - p = t\,d\theta/ds, \quad \text{where} \quad \sin\theta = dh/ds$$

and

$$\frac{dt}{ds} = -\frac{\mu}{h}(u_0 - u_1) + \frac{h}{2}\frac{dp}{ds}.$$

3.3.5. Non-dimensionalisation.
Lengths $\sim h_{\mathrm b} = 2q_0/u_0(1+\alpha)$, where $\alpha = u_1/u_0$ (from the flux equation with $dp/ds = 0$).

Independent variable: $S = s/h_{\mathrm b}$.

Dependent variables: $H = h/h_{\mathrm b}, \quad P = \dfrac{(p_0 - p)h_{\mathrm b}}{\mu u_0(1+\alpha)}, \quad T = \dfrac{t}{\mu u_0(1+\alpha)}$

$$\implies \quad \frac{d}{dS}\begin{pmatrix} P \\ T \\ H \\ \theta \end{pmatrix} = \begin{pmatrix} 6H^{-3} - 6H^{-2} \\ H^{-1}(2+4\alpha)/(1+\alpha) - 3H^{-2} \\ \sin\theta \\ P/T \end{pmatrix}. \tag{3.8}$$

– a system of ODE's.

3.3.6. Boundary conditions.
- $\theta = -\pi/2$ at $S = 0$ - where the theory fails!
- $\theta \longrightarrow 0$, $H \longrightarrow 1$ and $P \longrightarrow 0$ as $S \longrightarrow \infty$.
- $T(0)$ or $P(0)$ is given.

3.3.7. Numerical solution.
- Linearised analysis $\longrightarrow$ solutions in which H increases exponentially with both increasing and decreasing values of S. To avoid the solutions that "blow-up", integrate upstream from $S = \infty$. Give small perturbations to the downstream conditions and integrate until $\theta = -\pi/2$.
- Covered a range $25 < T(0) < 100$ and $|\alpha| \leq 1/2$, noting that the results are insensitive to these values of α.

3.3.8. Results. The numerical results (Fig. 34) can be summarised as follows:

1. The greatest pressure change occurs near O, which is consistent with lubrication theory.

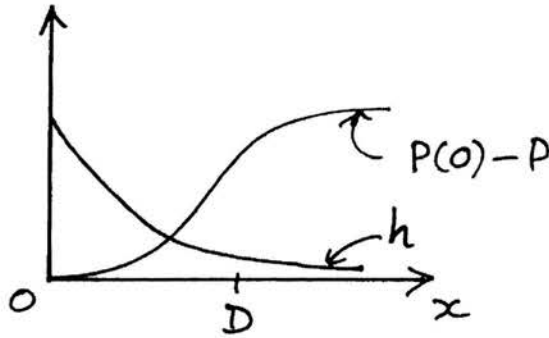FIGURE 34. Results of the numerical model for a 2D tank treading cell.

2. The tension does not change greatly between O and D: $T(D) \approx T(0)$ empirically.

3. Curve fitting to the numerical results gives, to within a few %:

$$H(0) = k_1[T(0)]^{k_2}, \tag{3.9}$$

$$P(0) = k_3[T(0)]^{1/3}, \tag{3.10}$$

where $k_1 = 0.925$, $k_2 = 0.571$ and $k_3 = 2.142$.

In dimensional variables,

$$b/h_0 = k_1[t(0)/\mu u_0(1 + \alpha)]^{k_2} \quad \text{at the lower gap,} \tag{3.11}$$

$$b/h_0 = k_1[t(0)/\mu u_0(1 - \alpha)]^{k_2} \quad \text{at the upper gap.} \tag{3.12}$$

4. Equation (3.10) gives h_a, h_b given p_0, α. To deduce p_0, α, integrate Eq. $(3.8)_2$ along the length of the cell and assume $t = t(0)$ at A, D and $t = 0$ at B and C to get

$$t(0) = \mu u_0 l_0(1 - \alpha)(1 + \lambda)/h_b,$$

$$t(0) = \mu u_0 l_0(1 + \alpha)(1 - \lambda)/h_a.$$

Thus we can deduce p_0, α given u_0 and λ.

3.3.9. Inaccuracy. Equation $(3.10) \implies p_0 = h_b^{-1} k_3 t^{1/3}(0) \left[\mu u_0 (1+\alpha)\right]^{2/3}$
for the lower gap with a similar expression at the upper gap. This

$$\implies \quad h_b/h_\alpha = \left(\frac{1+\alpha}{1-\alpha}\right)^{2/3} > 1.$$

But (3.11) (which comes from (3.9)) gives

$$\frac{h_b}{h_a} = \left(\frac{1+\alpha}{1-\alpha}\right)^{k_2}.$$

Assuming that these errors arise from the curve-fitting, the best thing is to average the two values geometrically.

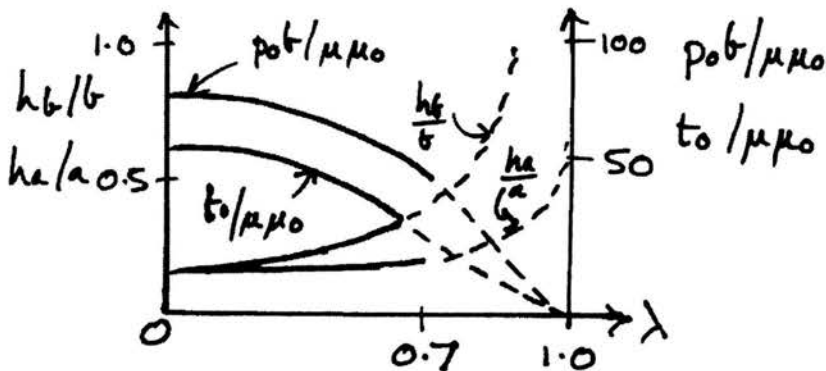**3.3.10. Results for α, p_0, h_a, h_b given l_0/b.** See Fig. 35.

FIGURE 35. The numerical results.

1. $\alpha \uparrow$ as $\lambda \uparrow$.

2. $h_b \uparrow$, $h_a \sim$ const. as $\lambda \uparrow$ until $\lambda > 0.7$ and $\alpha > 0.8$. The theory fails when $\lambda > 0.7$.

3. $p \downarrow$ as $\lambda \uparrow$ so dissipation decreases as λ increases $\implies$ that a natural system would tend to be asymmetric.

4. Consistent with observations.

   A fully 3-D model for a cell in a cylindrical tube was published by R. Hsu and T.W. Secomb [2]. The most recent work has concentrated on the non-uniformity of the capillary walls and the effects of glycocalyx lining the walls, e.g. white blood cells – a deformable solid rather than a fluid-filled sac whose shape is determined by the pressure distribution.

Acknowledgements

References

1. T.W. SECOMB *et al.*, Flow of axisymmetric red blood cells in narrow capilliaries, *J. Fluid Mech.*, Vol.163, pp.405–423, 1986.

2. R. HSU and T.W. SECOMB, Motion of nonaxisymmetric red blood cells in cylindrical capilliaries, *J. Biomech. Eng.*, Vol.111, pp.147–151, 1989.

3. H. TÖZEREN and R. SKALAK, The steady flow of closely-fitting incompressible elastic spheres in a tube, *J. Fluid Mech.*, Vol.87, pp.1–16, 1978.